On the imaging of stress changes in particulate media: an experimental study

J.C. Santamarina and B. Potts

Department of Civil Engineering, University of Waterloo, Waterloo, ON N2L 2V8, Canada

Received May 6, 1993

Accepted November 4, 1993

The stiffness of soils depends on the state of stress. Therefore, the velocity of wave propagation can be used to assess the state of stress and its changes. Indeed, given sufficient data, measurements can be inverted to produce a tomographic image of the stress field. A preliminary study of this approach was conducted with simulated data and is summarized briefly. Results of an experimental study are then presented. Three common geotechnical systems were tested: a footing, a moving surface load, and a retaining wall. Calculated velocity changes are compared with predicted velocity changes, with stress changes being estimated by classical analytical solutions. Good agreement is found in the three cases. The need for accuracy in travel-time measurements, difficulties in tomographic imaging, and the propagation of uncertainty from inverted velocities to stresses are discussed.

Key words: geophysical methods, tomography, wave propagation, stress, retaining wall, footings.

La rigidité du sol dépend de l'état de contrainte. En conséquence, la vitesse de propagation des ondes peut être utilisée pour évaluer l'état de contrainte et ses changements. En effet, avec une quantité suffisante de données, les mesures peuvent être inversées pour produire une image tomographique du champ de contrainte. Une étude préliminaire de cette approche conduite avec des données simulées est brièvement résumée. Les résultats d'une étude expérimentale sont alors présentés. Trois systèmes géotechniques courants ont été testés : une semelle, une charge mobile en surface, et un mur de soutènement. Les changements de vitesse calculés sont comparés aux changments de vitesse prédits au moyen de changements de contraintes qui sont évalués avec les solutions analytiques classiques. L'on trouve une bonne concordance dans les trois cas. Le besoin de précision dans les mesures du temps de parcours, les difficultés de l'imagerie tomographique, et la propagation de l'incertitude des vitesses inversées aux contraintes sont discutées.

Mots clés : méthodes géophyqiques, tomographie, propagation des ondes, contrainte, mur de soutènement, semelles.

[Traduit par la rédaction]

Can. Geotech. J. **31**, 215–222 (1994)

Introduction

The field of stress controls the performance of geotechnical systems. Yet stresses are usually estimated, and very seldom monitored. For example, stresses induced during construction around a single pile or groups of piles, the changes that take place during loading and mobilization of negative skin friction, and the relaxation of stresses with time are all major parameters in the design of pile foundations; however, little information is available on these phenomena. Other examples include monitoring the evolution of stresses around structures buried in saturated soils during earthquakes and determining the field of stress within the moving wedge prior to a landslide to properly compute its stability.

Monitoring interparticle forces or average stresses in a medium is difficult. The combined effects of relative stiffness and soil arching around transducers alter measurements, producing uncertain results. In addition, these are local measurements, and little can be inferred about the global field of stress in the medium.

Particulate media are governed by the effective state of stress. The higher the effective mean normal stress, the higher the strength according to Coulomb's failure criterion, and the higher the stiffness as predicted by Hertz's theory (White 1983). The propagation of mechanical waves depends on the stiffness of the medium, and its mass density. Hence, variations in stresses can be detected by wave-propagation techniques. In fact, if propagation data are obtained in different directions, i.e., illumination angles, it is possible to invert boundary measurements to obtain tomograms of the change in medium velocity. This picture can be further converted, by means of constitutive equations for the medium, to produce an image of the change in the field of stress.

Santamarina et al. (1993) presented results of a simulation study used to demonstrate the feasibility of using travel time of mechanical waves to generate a tomographic image of the state of stress in a medium. Three cases were considered, namely footing on a semi-infinite half space, plate load on a two-layer medium, and excavation within an infinite space. Induced stresses were computed with close-form solutions (Boussinesq, multilayer, and Kirsch), and local velocities were estimated by means of velocity–stress relationships, similar to those proposed by Roesler (1979). Tomographic travel-time data were artificially generated with a line integration algorithm assuming straight rays between sources and receivers. Finally, travel times were inverted with a tomographic program based on the ART algorithm. In the case of the Boussinesq problem, the image obtained after load application was subtracted, pixel by pixel, from the image obtained for the in situ state of stress. The resulting variation image clearly resembled the field of induced stress, as indicated in classical stress-bulb diagrams (Fig. 1) (after Santamarina et al. 1993).

The authors recognized several difficulties in the proposed methodology:

(1) Uneven distribution of information content within the imaged region. Some source–receiver configurations produce underdetermined regions. The worst case is the cross-hole configuration (see also Santamarina and Tallin 1993).

(2) Inherent anisotropy and vertical heterogeneity in wave velocities, which is the consequence of the anisotropic and heterogeneous field of stress in soils. In such a medium, paths of shortest travel time are not straight but curved.

(3) Diffraction of wave fronts when the wavelength λ is in the order of magnitude of the size of the velocity anom-

Printed in Canada / Imprimé au Canada

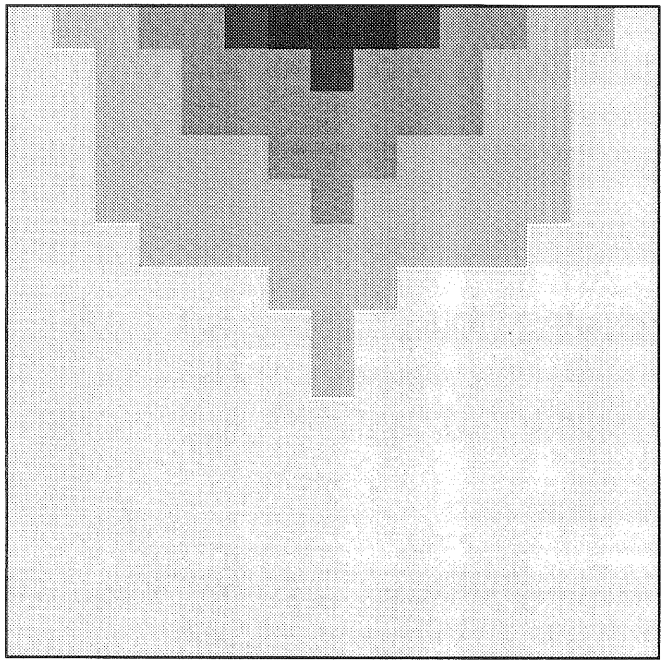

FIG. 1. Tomographic image of velocity variation under strip footing (simulated data, after Santamarina et al. 1993).

aly D_a. This is often the case for typical impact sources and geometry conditions involved in geotechnical studies. Under these conditions, ray assumptions lose validity, and diffraction must be taken into consideration. Furthermore, "diffraction healing" gradually restores the signal behind the anomaly to the free-field condition, making anomaly detection increasingly more difficult as the line of receivers moves farther away from the anomaly (Wielandt 1987; Potts and Santamarina 1993).

This paper reports results of an experimental study designed to gain further insight into the potential use of mechanical waves to assess the state of stress and the change in stresses in particulate media. Three geotechnical systems were modeled, namely a shallow foundation, a moving surface load, and a retaining wall. In the three cases, the location of instrumentation was selected to obtain "local" information, therefore minimizing difficulties listed above. Test conditions, materials, and instrumentation are described, followed by a discussion of observations.

General information

Sand

The experimental studies were conducted within a laboratory setting. Rounded quartz sand was used in all studies; its index properties are as follows: specific gravity G_s = 2.65, SiO_2 content 99.6%, median particle diameter D_{50} = 0.44 mm, coefficient of uniformity C_u = 1.5, coefficient of curvature C_c = 0.96, minimum void ratio e_{min} = 0.5, and maximum void ratio e_{max} = 0.74. Sand was placed by the dry-pluviation method; the opening size of the screen was fixed to control the rate of flow. A relative density of D_r 0.72 was obtained and had little or no variation between the raining heights h_{rain} = 180 mm and h_{rain} = 320 mm. This range of raining heights was used in all tests.

Constitutive equation

The nonlinear constitutive equation that relates velocity of compressional P waves to the state of effective stress for this sand was determined using a 27-L cubical triaxial. The device consists of six neoprene bladders connected in pairs to a three-channel control panel used to control pressure and to monitor volume changes in the three principal directions. The selected quartz sand was placed in the cubical triaxial by dry pluviation with a hopper, at the same relative density as used in the models. The regression analysis between the velocity (in m/s) of P waves, V_P, and the state of stress resulted in the following equations for loading

$$[1] \quad V_p = 359\left(\frac{\sigma_{prop}}{\sigma_{atm}}\right)^{0.22}, \qquad R^2 = 0.989$$

and unloading

$$[2] \quad V_p = 421\left(\frac{\sigma_{prop}}{\sigma_{atm}}\right)^{0.19}, \qquad R^2 = 0.926$$

where σ_{prop} is the normal stress in the direction of wave propagation and σ_{atm} is the atmospheric pressure, i.e., 1 atmosphere. Normal stresses perpendicular to the direction of propagation have no effect on the velocity of the propagating P wave (exponent less than ±0.01). The difference between the loading and unloading cycles characterizes the effect of prestraining and it is most significant at low preload ratios. Unloading data deviate from the straight line in log–log plots, i.e., lower coefficient of correlation.

Constitutive equations for shear waves relate velocity V_s to the stresses in the direction of propagation and in the direction of polarization. Thus, the combined use of P and S waves provides additional information about the state of stress, enhancing the potential of inversion algorithms. S waves must be used in the case of saturated media. Only P waves were monitored in this study.

Scale effects

The characteristic sizes of the tested systems were as follows: diameter of footing D = 0.228 m, diameter of moving load D = 0.228 m, and height of retaining wall H_{wall} = 0.80 m. The scale of these tests can be considered real size such as the imprint of car wheels, or reduced scale models in the case of footings and retaining walls. Following general guidelines in geotechnical modeling (balance between scale effects, stress history, and load-path difficulties), these one-gravity tests are appropriate models for structures within an order of magnitude larger scale. No scale effect is expected related to the ratio between the characteristic dimension of models and the size of sand grains ($D_{plate}/D_{50} \approx 500$; $H_{wall}/D_{50} > 1600$). Boundary effects were present and are discussed in the text. Wherever possible, results are presented in dimensionless terms.

Instrumentation

The instrumentation used to measure wave velocities was similar in all tests. Small piezoelectric transducers were used as sensors (12 mm diameter and 1 mm thickness); they were buried in the sand during pluviation, and their location was carefully corroborated before sand pluviation continued. Small "hammer and plate" impact sources were used from the surface of sand beds, as well as from the sides of sand boxes. Given the small size of models, the uncertainty in the location of sources and receivers can account for ≤5% error in measured velocities.

Signatures were recorded with a PC-based multichannel digital storage oscilloscope sampling at 500 kHz per chan-

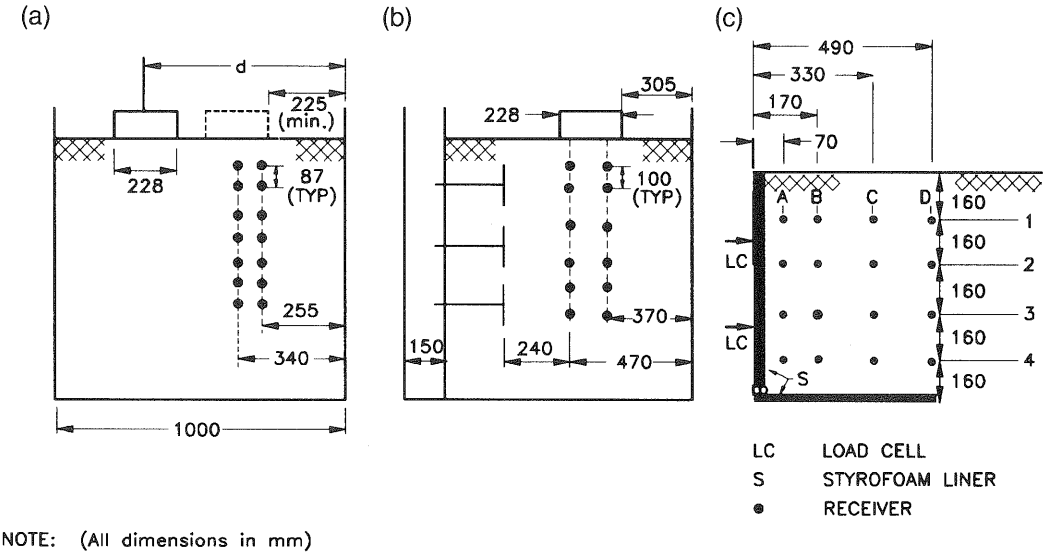

FIG. 2. Experimental settings. All dimensions are given in millimetres.

nel. Travel times were manually determined from the screen as the difference between the initiation of the signature detected at consecutive receivers. Measured travel times varied between 0.2 and 3 ms. The frequency of first arrivals remained between 3000 and 5000 Hz, allowing for a precision in the determination of first arrivals in the order of 10 μs. Therefore, the estimated error on measured travel times is ±5% for short distances and less than ±1% for long ones. Finally, although sensors were accurately located during construction, no correction for the variation in the position of sensors during testing was done; given the observed boundary deformations and assuming typical strain influence diagrams, it is estimated that changes in the relative location of two consecutive transducers is less than 3% of the distance between them, in all cases. This error is comparable with other measurement errors in this study.

Experiment 1: shallow foundations

The computation of the settlement of footings on sands faces several difficulties, including the immediate change in the field of stiffness in the sand upon the application of the load (this is not the case in the immediate settlement of footings on saturated clays). The purpose of this experiment is to measure, by means of wave propagation, the change in the field of stiffness and therefore the field of stress underneath footings.

Two plate load tests were conducted in a 1 m^3 cubical steel box, constructed from bolted channel sections with smooth internal walls. Vertical velocities were measured in test 1 (set up similar to that shown in Fig. 2*a*) and horizontal velocities in test 2 (set up shown in Fig. 2*b*). Load was applied with a hydraulic jack bolted to a reaction frame attached to the box. The pressure gauge on the jack was calibrated using a standardized load cell. The footing was loaded to failure in both tests. All necessary measurements were taken at convenient stable intervals.

The instrumentation was similar in both tests and consisted of two vertical lines of piezoelectric sensors buried in the sand bed during pluviation. In test 1, the plate was centred directly over one column of sensors ($r/R = 0$, where r is the radial distance from the centre of the plate, and R is the radius of the plate); the second column was offset radially by 87 mm

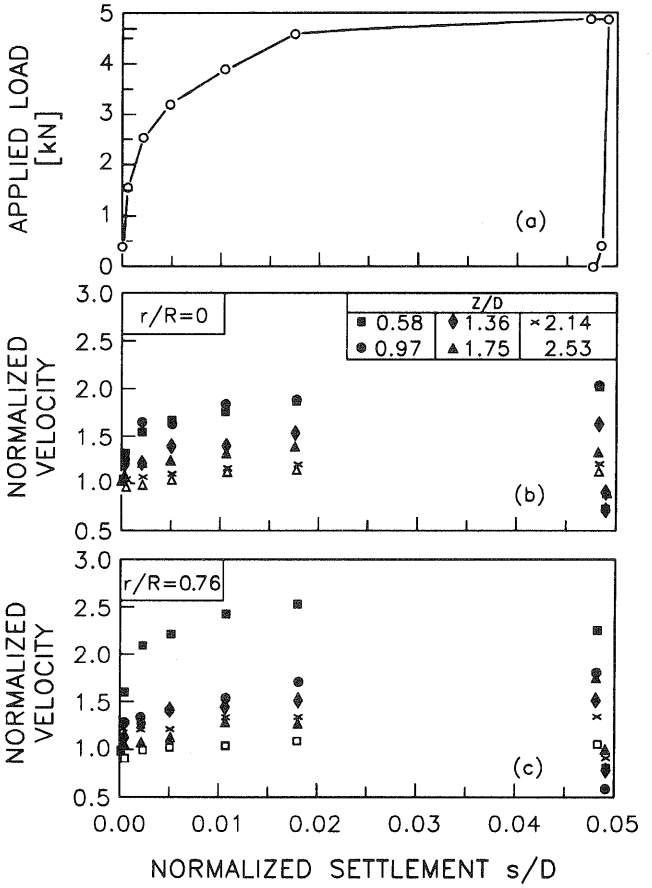

FIG. 3. Plate load test. Vertical velocity vs. settlement.

($r/R = 0.76$). Piezoelectric transducers were placed every 87 mm in depth starting 87 mm beneath the initial surface of the sand. The closest boundary was 225 mm from the edge of the plate. In test 2, the two columns of receivers straddled the centre line of the footing. Spacing of the receivers was at 100 mm, and the closest boundary was 305 mm from the plate. A bulkhead was placed in the sand box, 150 mm away from one wall; horizontal impact sources were mounted on the bulkhead and buried in the sand during pluviation.

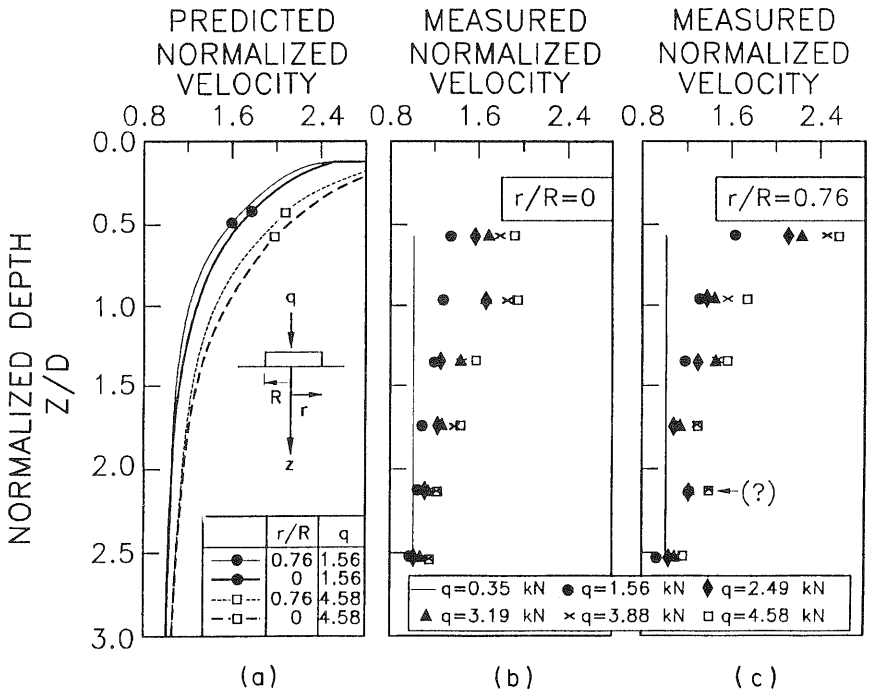

FIG. 4. Plate load test. Measured and predicted vertical velocity vs. depth.

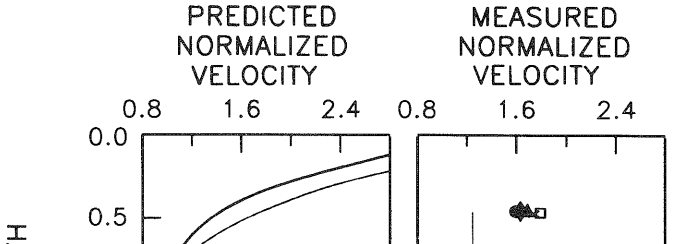

FIG. 5. Plate load test. Measured and predicted horizontal velocity vs. depth.

Figure 3 shows results from test 1. The applied load and normalized vertical velocity under the centre line and at $r/R = 0.76$ are plotted as a function of the settlement s normalized with respect to the plate diameter D, s/D. Figure 3*a* shows the load–displacement curve for the test, Fig. 3*b* shows normalized velocity under the centre line for six different values of z/D (where z is depth measured from the initial surface), and Fig. 3*c* presents similar data for the off-centre location at $r/R = 0.76$. All trends are similar: vertical velocity increases with applied load in all cases; and the shallower the observation depth, the higher the velocity increase.

Figure 4 shows measured and predicted values of vertical velocity with depth. Velocities are normalized with respect to the initial velocity before load application; depth is normalized with respect to the plate diameter (z/D). Figure 4*a* shows values of velocity computed with [1], taking into consideration the in situ stress and the induced state of stress. Induced stresses were calculated with Boussinesq's solution for circular plates. Figures 4*b* and 4*c* show normalized measured values for the two lines of receivers ($r/R = 0$ and $r/R = 0.76$). The normalization velocity was taken when a nominal load was applied on the footing.

There is good agreement between measured vertical velocities and those predicted with stresses estimated from theory of elasticity; this is true even when the applied load approaches failure. The normalization with measured velocities before loading V_o enhances the effect of discrepancies and errors at shallow depths where V_o is very low. Measured velocities are average values of velocities between the location of sensors, and in the case of vertical propagation this results in overestimation of the velocity at shallow depths. High normalized velocities at $z/D = 2.2$ and $r/R = 0.76$ are likely the result of a low initial velocity used for normalization, and therefore would not have any phenomenological implication. A similar justification could explain normalized velocities less than 1.

The agreement between measured and predicted velocities is better for the off-centre measurements ($r/R = 0.76$). The most significant difference between measured and predicted velocities takes place under the centre line, for depths shallower than $z/D = 1.0$, and for loads q that exceed $q = 1.56$ kN. It is observed that the velocity does not continue increasing, indicating a constant stress level. From Fig. 3, $q = 1.56$ kN corresponds to a factor of safety against bearing capacity $FS_{bc} \approx 3$. Finite element solutions with elastoplastic models predict the beginning of significant yielding under

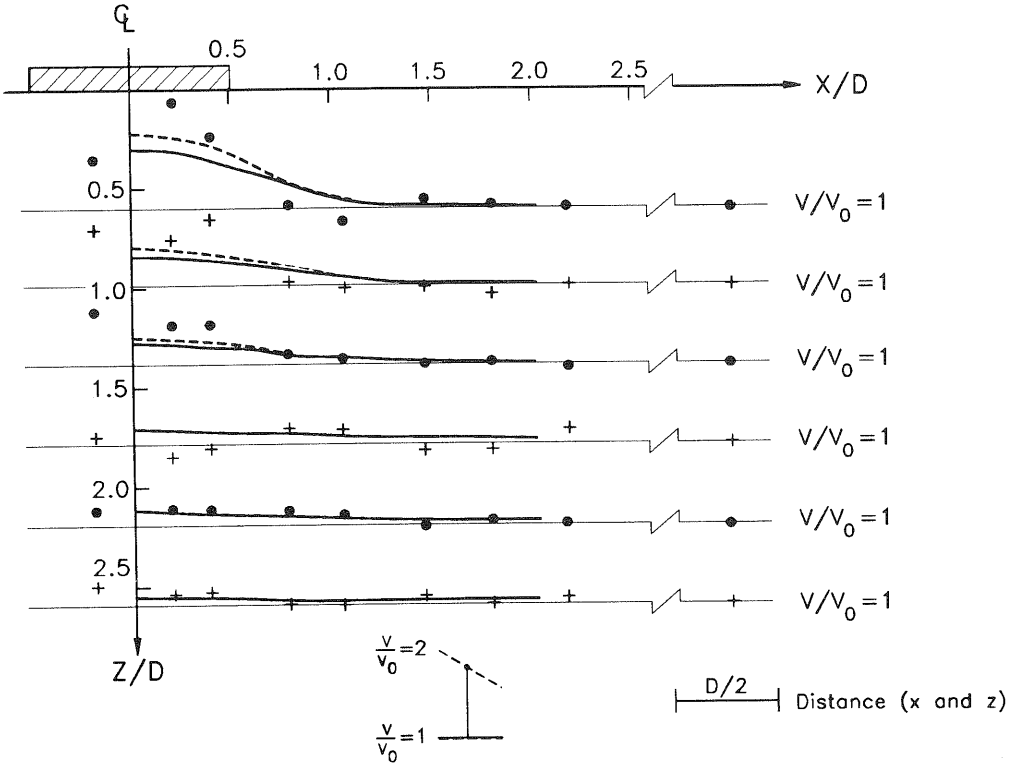

FIG. 6. Moving load. Velocity at different relative positions.

the centre line at $z/D = 0.5$, and at factor of safety FS $\leq$ 3. In addition, it is known that the distribution of contact pressure underneath footings on granular materials is a function of the load (Terzaghi 1943; Ranganatham et al. 1973; Hartikainen 1973).

Figure 5 shows measured and predicted values of normalized horizontal velocity with depth. Figure 5*a* shows values computed from theory of elasticity, and Fig. 5*b* shows measured values under the centre line, normalized with respect to horizontal velocities obtained with a nominal load on the footing. Horizontal velocities are in agreement for the lowest load. Differences between predicted and measured velocities increase for higher loads and for depths in excess of $z/D = 0.5$. This is in agreement with results by Ahtchi Ali (1992), who studied the effect of boundaries on the deformation and ultimate capacity of model footings in a sand box and observed that the effect of boundaries increases with the load, or normalized settlement. The velocity data show that the low ratio between the size of the box L and the size of the plate D, $L/D = 4.4$, leads to significant increase in horizontal stress at high normalized settlement. Horizontal velocities estimated from the horizontal stress at no-lateral strain ($\epsilon_h = 0$) are in good agreement at $z/D = 1.36$.

Experiment 2: quasi-static moving loads

Ray bending is one of the most significant difficulties in geotechnical tomography. This is predominant in soils because of their inherent heterogeneity and anisotropy. In the case of moving loads, travel times can be measured along a line of sensors for different locations of the moving load. This is identical to the case of a static plate and multiple lines of receivers. The result is local values of velocity at different depths and at multiple relative distances from the load. A pixel image can then be created by coloring pixels with the measured values. Although this image resembles a tomogram, it is generated without inversion, requires a small number of receivers, and involves minimum uncertainty related to ray-path linearity. The proposed approach is applicable in space-invariant cases where changes in space keep a strong correlation with changes in time; stresses induced by vehicular load are a classical civil engineering example (first suggested by K. Stokoe, University of Texas at Austin).

This test was conducted on a sand bed deposited in the same steel box used in experiment 1, with identical location of receivers (Fig. 2*a*). The circular plate, diameter D = 0.228 m, was placed on the soil surface and loaded with a hydraulic system to a preselected load q = 2.22 kN (load fluctuations of 10% were observed during the test). Vertical travel times were measured along the two vertical lines of sensors. The footing was then unloaded and moved to a new position aligned with the previous one and the location of the receivers.

The footing was positioned in six different locations, and a total of three different passes were made; the data became increasingly more consistent with each pass. It is expected that the position of shallow sensors was altered in subsequent passes; however, final locations were not determined. The most significant change was the densification of the upper layers, which leads to a reduction of the distance between the plate and the first receiver. On the basis of theory of elasticity, a maximum error of 12% is expected in the state of stress for a change in distance of approximately 2 cm.

Computed local velocities between contiguous receivers i and $i + 1$ were normalized with respect to measured velocities before load application (i.e., footing "far" from instrumented plane). Normalized velocities are plotted at the intermediate depth $z = (z_i + z_{i+1})/2$, and at distance x which corresponds to the horizontal distance between the centre

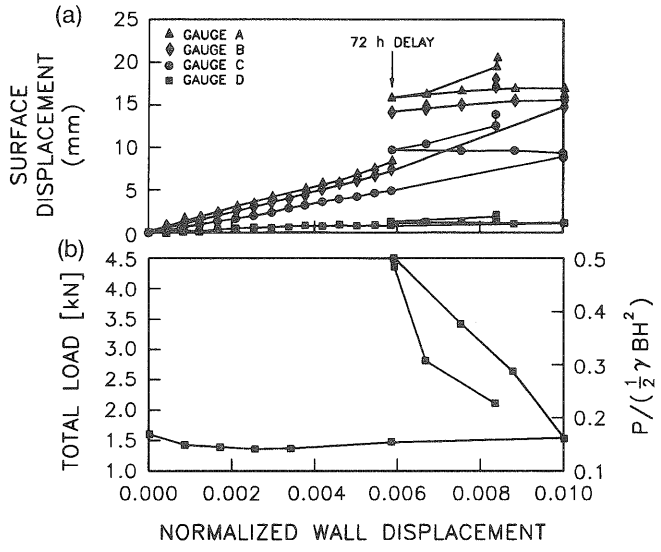

FIG. 7. Retaining wall. Load and deformation.

of the plate and the line of receivers. The compilation of data for all locations of the plate yields a complete picture of the field of vertical velocity (Fig. 6). Velocities computed with induced stress assuming theory of elasticity are shown as lines (continuous line for the original elevation of the sand surface, and broken line for the observed elevation at the beginning of the third pass).

These data are less consistent than values presented in previous figures. However, it is important to recognize that data from multiple load–unload–move cycles are superimposed on the same figure, and that the normalization of measured velocities accentuates experimental errors. Measured velocities follow trends similar to those of velocities predicted assuming theory of elasticity. The most significant deviation from theoretical trends takes place at shallow layers and low horizontal offset ($z/D < 1$ and $x/D < 0.5$), where measured velocities are significantly higher than predicted velocities. Unfortunately, there is no assurance as to the alignment of the source and the receivers when the footing is placed on top of the strings of receivers. Misalignment leads to late triggering of the oscilloscope and shorter measured travel times, which particularly affect the shallower receivers.

Experiment 3: retaining wall

The purpose of this study was to evaluate the potential use of mechanical waves in the investigation of the state of stress in retained fills. This study was conducted with a rectangular sand box built within a reaction frame. The side acting as the retaining wall was $H = 0.8$ m high and $B = 1.6$ m wide. This ratio $B/H = 2$ is referred to as the Terzaghi criterion and was adopted in early geotechnical work to minimize the effect of side boundaries on measurements conducted on the central plane. Later experimental and numerical work showed $B/H = 2$ insufficient (Azzouz and Baligh 1975; Lyndon and Schofield 1978; Santamarina and Goodings 1989). For the purpose of this study, boundary effects are not critical; in fact, the study of boundary effects is an application of the proposed approach.

The front wall was vertically supported on rollers and horizontally restrained by four calibrated load cells that were mounted on the reaction frame, at the one-third points of the wall panel. Millimetric adjustment screws on the load cells were used to control the movement of the wall; the horizontal displacement was also monitored on both boundaries by means of dial gauges. The displacement of the top surface was monitored with four dial gauges. Styrofoam sheets, 12 mm in thickness, were placed immediately behind the retaining wall and on the base of the box to minimize the effects of refraction on the measurement of travel times along the "A" and "4" lines in Fig. 2*c* (refracted signals were not observed).

Impact sources were activated on the top surface and on the retaining wall, and wave arrivals were detected by means of 16 piezoelectric sensing elements mounted on the central plane during sand pluviation (Fig. 2*c*). The horizontal spacing of sensors was selected to gain insight into velocity variations across the hypothetical active failure plane, while maintaining definition behind the wall. The vertical spacing was constant. The positioning of sensors was within 2 mm accuracy.

After construction and instrumentation, a complete set of initial readings were conducted. The test consisted of three stages: (1) gradual movement of the wall away from the retained fill, mobilizing active resistance; (2) movement against the fill, partially mobilizing the passive resistance; and (3) outward movement. Stage 3 was conducted 72 h after the completion of stage 2. The passive cycle was not intended to fully mobilize passive resistance, as the size of the box was not designed to accommodate the formation of the passive wedge; instead, the objective was to provide further information on the sensitivity of travel-time measurements to the changes in effective stresses.

The evolution of boundary parameters (i.e., surface deformations and loads) and internal parameters (i.e., velocity) was monitored at multiple stages. Figure 7*a* shows the displacement of the top surface as a function of the horizontal wall displacement δ_h/H. The surface displacement is significant for gauges at positions A ($x/H = 0.09$) and *B* ($x/H = 0.21$), decreases towards position C ($x/H = 0.41$), and is minimum at position D ($x/H = 0.61$). Volume computations at the end of the first active phase show an average net dilatancy of $\Delta V/V_o \approx 0.4\%$ for the active wedge.

Figure 7*b* shows the total horizontal force measured by the four load cells as a function of the horizontal wall displacement $\delta h/H$. Data are also presented in dimensionless form on the secondary *y* axis; this π ratio is equivalent to the average coefficient of earth pressure. The initial load is significantly lower than the value expected for a condition of no lateral strain (for $\phi = 41°$, $k_o = 0.34$, where ϕ is the angle of internal friction, and k_o is the ratio of horizontal to vertical effective stress at no lateral strain). Given that minimum side and base boundary effects are expected at no lateral displacement of the wall (Vargin 1967; Lazebnik and Chernysheva 1968), it is concluded that the low measured value results from the relaxation during construction of the 12 mm styrofoam sheet placed behind the wall. The most significant observation during the first four stages of wall movement was the extreme sensitivity of measured loads in each load cell with the deformation pattern imposed on the wall during displacement. Horizontal velocities also denounced this effect, indicating stress changes as high as 100%. The parallel, even movement of the wall was carefully implemented in all subsequent stages.

Figure 8 shows the variation of average vertical velocities between sensors at elevations 1 and 4, at locations A–D.

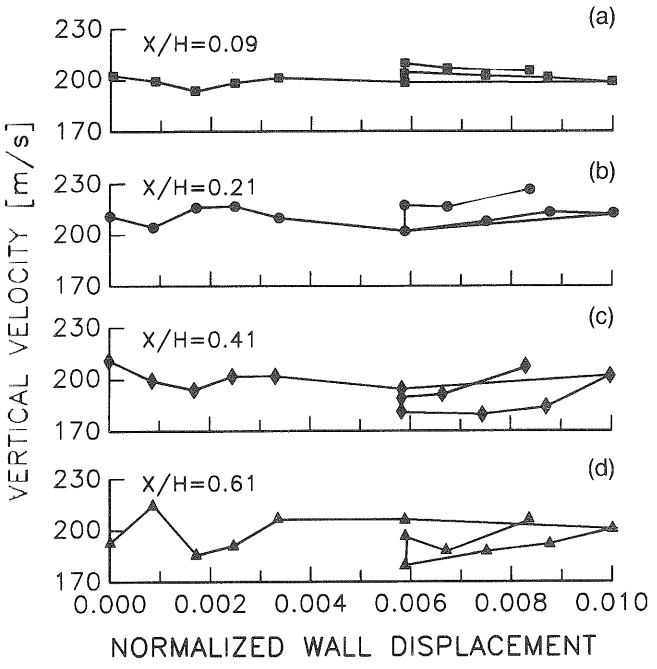

FIG. 8. Retaining wall. Average vertical velocity between sensors at locations 1 and 4, at all four locations (a–d).

There is no conclusive trend during the first active stage. During the passive stage, the "average" vertical velocity decreases at locations B, C, and D (at x/H = 0.21, 0.41, and 0.61, respectively), indicating a significant reduction in the average vertical stresses. At the same locations, the average vertical velocity increases during the last active stage, but not as significantly as before.

The vertical velocity increases at all locations during the 72 h delay between the passive phase and the second active phase. The effect of time-dependent processes may be twofold: it may have a direct effect on the propagation of waves (certainly on attenuation) at constant stress, and it may alter the field of stress, indirectly affecting wave propagation. We have observed time effects on wave propagation in clays during secondary compression. The discrimination of the two components listed above is under study.

Average horizontal velocities between A and D receivers at all four elevations are presented in Fig. 9 (same velocity scale as Fig. 8). These data show significant changes in horizontal velocities, and therefore horizontal stresses behind the retained fill. Nonstable measurements are observed in the earlier stages of wall movement, in agreement with load-cell measurements as explained before. The highest sensitivity to wall displacement is observed at z/H = 0.4 (elevation 2). This trend is similar to the horizontal load measured with load cells (Fig. 7*b*). At this elevation, the decrease in horizontal velocity during the first active stage indicates stress changes twice as high as those predicted by the k_o/k_a ratio (where k_o is the ratio of horizontal to vertical effective stress at no lateral strain, and k_a is Rankine's active earth pressure coefficient). During the passive stage, the horizontal velocity increases significantly, from 85 to 175 m/s. According to [1], this increase in velocity indicates an increase in horizontal stress by a factor of 26. For reference, the ratio of horizontal stress between the passive and the active Rankine states can be estimated as $k_p/k_a = k_p^2$ (since $k_p = 1/k_a$); this ratio is 21 for $\phi = 40°$ and 28 for $\phi = 43°$. This variation in

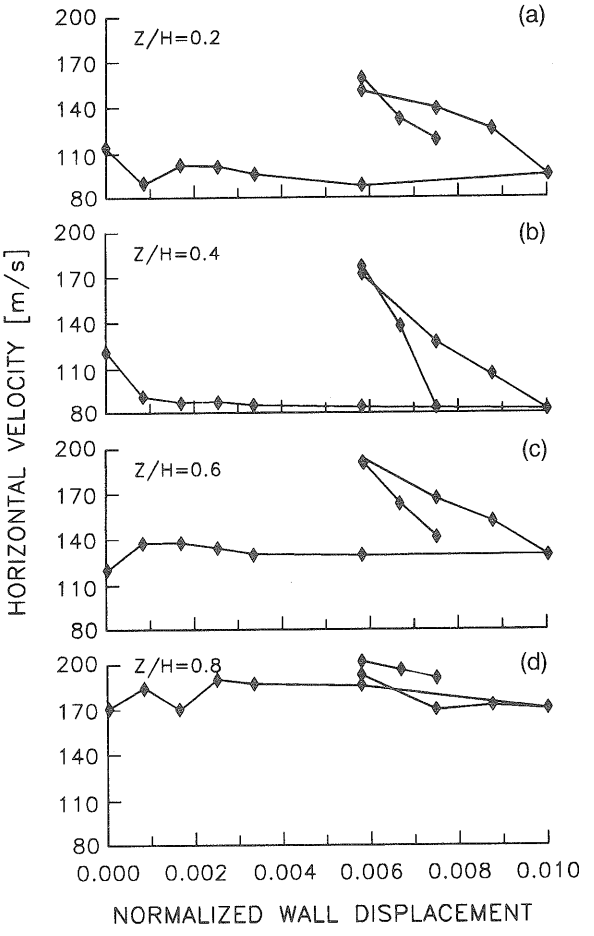

FIG. 9. Retaining wall. Average horizontal velocity between sensors at locations a and d, at all four elevations (1–4).

angle of internal friction corresponds to changes in dilatency at shallow depths. Boundary effects along side and back walls favor higher stresses than the ideal Rankine passive case; however, the amount of wall displacement (δ/H = 0.4%) and the load–deformation diagram in Fig. 7 indicate that full mobilization of passive resistance was not achieved.

Measurements with the lowest string of receivers, z/H = 0.8, shows little sensitivity to wall displacement. It is known that the effect of friction along the lower boundary restricts changes in the state of stress in this region. This effect has been recognized in retaining-wall design and is often taken into consideration as a reduction of pressure on the wall.

From velocity to stress

Constitutive equations

When significant shear planes form, the interpretation of velocity data may need further evaluation (eqs. [1] and [2] are valid for stress ratios between 1:3 and 3:1). Furthermore, significant attenuation takes place in regions that approach failure, and the detection of first arrivals becomes difficult; then, measured travel times reflect unwanted combinations of attenuation and velocity fields.

Variations in void ratio that accompany contractive and dilative processes have second-order effects on the velocity of propagation in particulate media. These effects are partially incorporated in constitutive relations, such as [1] and [2]. The monitoring of porosity changes as an indicator of stress changes is relevant in X-ray tomographic studies,

or in the geophysical exploration of deep sediments in reference to petroleum geomechanics.

Propagation of uncertainty

Constitutive equations [1] and [2] are of the form $V = b\sigma^c$ where b and c are constants. If the distribution of velocity and stress are both considered log normal, then the standard deviation S of the logarithm of the estimated stress, $\log \sigma$, is related to the standard deviation of the logarithm of the measured velocity, $\log V$, as

$$[3] \quad S_{(\log \sigma)} = \frac{1}{c} S_{(\log V)}$$

Given that typical c values are about 0.20–0.25, the propagation of uncertainty from measured velocities to stresses is considerable and must not be overlooked. High-frequency sources, proper triggering, and adequate determination of arrivals are required. Results presented in this study were compared in terms of velocity.

Conclusions

The dependency of wave velocity on the state of stress in particulate media permits monitoring stress changes by wave-propagation techniques. Adequate constitutive equations can be determined in the laboratory. Because of the form of these equations, the uncertainty in measured velocities is magnified on the inverted stresses. Therefore, accurate determination of travel times is required; the use of high-frequency sources is recommended.

Experimental data were presented for three geotechnical systems, namely footing, moving surface load, and retaining wall. In all cases, results show good agreement with predictions based on classical close-form solutions. Measurements detected yielding and the effect of boundaries.

Given sufficient boundary measurements, the tomographic image of the state of stress in the enclosed region can be reconstructed. Inversion algorithms based on nonlinear rays are required, and the position of sources and receivers must be properly selected to optimize the distribution of information content within the region under study.

Acknowledgments

Figure 1 was reprinted with permission given by the Transportation Research Board, National Research Council, Washington, D.C. K. Bowman helped in the design and construction of all test settings. K. Klein, D. Reeves, J. Caron, and J. Wu, participated in the testing of the retaining wall. This study was supported in part by the Natural Sciences and Engineering Research Council of Canada and Turkstra Lumber. The authors are grateful to the reviewers for their useful comments.

Ahtchi Ali, F. 1992. An experimental study of settlement of footings on sands (penetration and geophysical testing). Ph.D dissertation, Polytechnic University, Brooklyn, N.Y.

Azzouz, A.S., and Baligh, M.M. 1975. End effects on the stability of cohesive slopes. ASCE Journal of the Geotechnical Engineering Division, **101**: 1105–1117.

Hartikainen, J. 1973. On the distribution of the vertical and horizontal contact pressure components under a rigid foundation. *In* Proceedings, 8th International Conference on Soil Mechanics and Foundation Engineering, Moscow, Aug. 6–11, 1973. Vol. 1, pp. 99–105.

Lazebnik, G.E., and Chernysheva, E.I. 1968. Certain errors in the experimental determination of earth pressure on models of retaining walls (Discussion), Hydrotechnical Construction (USSR), pp. 333–339.

Lyndon, A., and Schofield, A.N. 1978. Centrifugal model tests on the Ladalen landslide. Canadian Geotechnical Journal, **15**: 1–13.

Potts, B.D., and Santamarina, J.C. 1993. Geotechnical tomography: the effects of diffraction. ASTM Geotechnical Testing Journal, **16**: 510–517.

Ranganatham, B.V., Rengaraju, V.R., and Sivasundara Pandian, N. 1973. Contact pressure beneath R.C. test footings. *In* Proceedings, 8th International Conference on Soil Mechanics and Foundation Engineering, Moscow, Aug. 6–11, 1973. Vol. 1, pp. 209–212.

Roesler, S.K. 1979. Anisotropic shear modulus due to stress anisotropy. ASCE Journal of the Geotechnical Engineering Division. **105**: 871–880.

Santamarina, J.C., and Goodings, D.J. 1989. Centrifuge modeling: a study of similarity. Geotechnical Testing Journal, **12**: 163–166.

Santamarina, J.C., and Tallin, A. 1993. Image enhancement in geotomography. *In* Proceedings of a Conference on Digital Image Processing: Techniques and Application in Civil Engineering Kona, Hawaii, Feb. 28–March 5. *Edited by* D. Frost and J. Wright. American Society of Civil Engineers, New York, pp. 246–254.

Santamarina, J.C., Graham, J., MacDougall, C., and Roy, V. 1993. Tomographic imaging changes in effective stress in granular media (simulation study). Transportation Research Records, No. 1415, pp. 95–99.

Terzaghi, K. 1943. Theoretical soil mechanics. John Wiley & Sons, Inc., New York.

Vargin, M.N. 1967. Influence of the side walls of an experimental tray on the measured soil pressured. Soil Mechanics and Foundation Engineering (USSR), pp. 247–249.

White, J.E. 1983. Underground sound. Elsevier Science Publishing Co., Inc., New York.

Wielandt, E. 1987. On the validity of ray approximation for interpreting delay times. *In* Seismic tomography. *Edited by* G. Nolet. Reidel Publishing Company, Boston, pp. 85–98.